Journal of Applied Physics ARTICLE scitation.org/journal/jap

Enhanced performance of an Ag(100) photocathode by an ultra-thin MgO film

Cite as: J. Appl. Phys. **132**, 195303 (2022); doi: 10.1063/5.0124528
Submitted: 6 September 2022 · Accepted: 25 October 2022 ·
Published Online: 16 November 2022

C. Benjamin,[1,a)] H. M. Churn,[2,b)] T. J. Rehaag,[1] L. A. J. Soomary,[3,b)] C. P. Welsch,[3] L. B. Jones,[2,b)] T. C. Q. Noakes,[2,b)] and G. R. Bell[1]

AFFILIATIONS

[1]Department of Physics, University of Warwick, Coventry, United Kingdom
[2]ASTeC, STFC Daresbury Laboratory, Warrington, United Kingdom
[3]Department of Physics, University of Liverpool, Liverpool, United Kingdom

[a)]**Author to whom correspondence should be addressed:** Christopher.Benjamin@stfc.ac.uk. **Also at:** ASTeC, STFC Daresbury Laboratory, United Kingdom.
[b)]**Also at:** Cockcroft Institute of Accelerator Science, Daresbury, United Kingdom.

ABSTRACT

Metal photocathodes are widely utilized as electron sources for particle accelerators for their ease of use, high durability, and fast response time. However, the high work function (WF) and low quantum efficiency (QE) typically observed in metals necessitate the use of high power deep UV lasers. Metal oxide ultra-thin films on metals offer a route to photocathodes with a lower WF and improved QE while maintaining photocathode durability and response time. We show how the photocathode performance of an Ag (100) single crystal is enhanced by the addition of an ultra-thin MgO film. The film growth and WF reduction of 1 eV are characterized, and the QE and mean transverse energy (MTE) are measured as a function of illumination wavelength. An eightfold increase of QE is achieved at 266 nm without adding to MTE through additional surface roughness, and the resistance of the photocathode to O_2 gas is greatly improved.

I. INTRODUCTION

Next-generation electron sources for particle accelerators place increasingly stringent demands on the photocathode used for initial charge generation. Photocathodes must show high quantum efficiency (QE), low intrinsic emittance, fast temporal response, and long lifetime. The intrinsic emittance is defined as the position and energy spread of the photoemitted particle bunch in the three orthogonal axes and the QE is defined as the ratio of the number of electrons emitted to the number of incident photons. Depending on the accelerators application, the photocathode requirements can vary. For example, x-ray free electron lasers require high brightness beams, while ultra-fast relativistic electron diffraction and microscopy requires high coherence, low beam emittance, and a very short pulse width. In both cases, low intrinsic photocathode emittance is required for high beam brightness as poor beam emittance cannot be compensated for further along the accelerator.[1] Consequently, the photocathode defines the lower limit of the achievable beam emittance, thus highlighting the importance of the photocathodes intrinsic emittance. Direct measurement of these parameters, including comprehensive analysis, is therefore critical as part of the development of new photocathode materials. The photoemissive properties are predominantly governed by the surface characteristics of the photocathode. The surface roughness (r_a) and the work function (WF) strongly influence both the QE and intrinsic emittance.[2]

The intrinsic emittance is measurable as its mean transverse energy (MTE). MTE is a photoemissive property of the cathode which is dependent on multiple factors: the surface roughness of the cathode,[3] external field incident to the surface, and the excess energy in the photoemission process. In an ideal case, where surface roughness contribution is negligible, the MTE can be

modeled by just the effect of the excess energy following the Dowell–Schmerge approximation

$$\mathrm{MTE} = \frac{1}{3}(h\nu - \phi), \tag{1}$$

where $h\nu$ is the incident photon energy, ϕ the photocathode WF, and $(h\nu - \phi)$ corresponds to the excess energy of the photoelectron.[4,5]

Metal photocathodes are predominantly employed for their ease of use, high durability, and fast response time. However, the high WF and low QE typically observed in metals necessitate the use of high power deep UV lasers, involving harmonic conversions and pulse shaping; such optical requirements add complexity and cost.[6] First-principles calculations have shown that metal oxide films on metals can produce a surface with a lower WF.[7,8] This significant WF reduction is induced by a strong dipole moment at the metal oxide/metal interface. The dipole moment has been shown to have three contributing factors: interfacial charge transfer, electrostatic compression, and surface reconstruction mechanisms.[9] This has also been demonstrated experimentally with ultra-thin MgO films on Ag(100).[10]

MgO is a wide bandgap material (7.8 eV) with a high photon transmission all the way to deep UV wavelengths. Thus, an ultra-thin MgO film has the potential to reduce the WF of the metal photocathode while impeding neither UV photon absorption in the underlying metal nor low energy electron emission into the vacuum. Such a WF reduction should increase the QE across the mid-UV spectrum. Coupled with its high thermal and chemical stability,[11] MgO also has the potential of increasing the robustness of the photocathode by preventing degradation of the more reactive underlying metal surface through contamination by residual vacuum gases.

This latter property is likely to be important for photocathodes operating at high pressure, for example, in gaseous electron multiplier (GEM) structures.[12,13] A robust photocathode with good QE in the mid-UV range would be suitable for a range of sensing applications, such as water quality monitoring.[14] The lifetime of an oxide-terminated photocathode in a sealed GEM cell should be greatly improved over a more reactive surface.

In this work, we demonstrate all of these attributes for ultra-thin MgO films grown on clean Ag(100) single crystal surfaces. A reduction of WF close to 1 eV was achieved, corresponding to an increase of QE by a factor of 8 at 266 nm. The increase of MTE was minimized since the surface roughness of the photocathode was not worsened by MgO film growth, and the MgO/Ag(100) photocathode was more resistant to QE degradation on exposure to oxygen.

II. METHODS

Sample preparation and *in situ* characterization were carried out in a customized VG multiprobe ultra-high vacuum (UHV) system, with a base pressure of 3×10^{-9} mbar. This characterization included QE measurement, x-ray and ultraviolet photoelectron spectroscopy (XPS, UPS), and low energy electron diffraction (LEED). *Ex situ* investigation included atomic force and lateral force microscopy (AFM, LFM) in ambient air, and MTE measurements in a separate system via UHV suitcase transfer.

A. Sample preparation

A 6 mm diameter Ag(100) cathode was supplied by Surface Preparation Laboratory (Netherlands), polished to a $r_a < 30$ nm. The crystal was cleaned in the UHV system using cycles of 2 keV Ar^+ bombardment and annealing at 600 °C.[15] The MgO ultra-thin film was deposited by the thermal evaporation of Mg from a calibrated Knudsen effusion cell with the Ag crystal in an O_2 partial pressure of 5×10^{-7} mbar. The Ag crystal temperature (T_s) was 300 K during deposition.

B. Surface characterization

XPS spectra were obtained using a non-monochromated Al K_α x-ray source (1486.7 eV) and a Thermo Alpha 110 hemispherical electron energy analyzer. The analyzer transmission function was determined experimentally using the technique described by Ruffieux *et al.*,[16] and the effective WF (4.26 eV) of the analyzer was calibrated using the Fermi edge of Ag. Survey and core region spectra were acquired with a pass energy of 50 and 20 eV, respectively. XPS data analysis was conducted using the CasaXPS software package.[17] UPS spectra was obtained for the MgO/Ag(100) film, using a He discharge lamp (21.2 eV), extracting the work function by measuring the low kinetic energy cutoff and the Fermi edge. *Ex situ* AFM and LFM measurements were conducted in ambient air. Both contact (LFM) and peakforce tapping (roughness) mode measurements were conducted on a Bruker Dimension Icon after all previous work was conducted.

C. Photoemissive characterization

Absolute QE (QE_{ab}) measurements were made in the multiprobe chamber using a Crylas FQSS Q4 266 nm, 1 kHz pulsed laser source coupled with a ×3 beam expander and 2 mm circular aperture, and then a 2.0 OD reflective filter yielding an optical power of 1.16 μW illumination on the sample. A high voltage extraction electrode was placed close to the sample and a lock-in amplifier was used to measure the total yield photocurrent, thus extracting the true photocurrent, with an error of ±7%, free from DC background and with reduced noise.

Once prepared and characterized, the photocathode samples were transferred to the transverse energy spread spectrometer (TESS) under ultra-high vacuum (UHV) conditions ($<10^{-10}$ mbar) via a vacuum suitcase transfer. TESS captures the photoemission footprint of a photocathode under illumination from deep-UV to infrared wavelengths.[18] The transverse energy distribution curve (TEDC) is extracted from the photoemission footprint, and the mean transverse energy (MTE) was determined from the TEDC.[19,20]

III. RESULTS

A. Surface characterization

The cleanliness and crystallinity of the Ag(100) surface were confirmed using XPS and LEED. After the final cleaning cycle, XPS

TABLE I. Peak fitting parameters for the core region spectra from the substrate before and after MgO film deposition. The Auger parameters are also shown.

	Core region	Peak position (eV)	FWHM (eV)
Substrate	Ag $3d_{5/2}$	368.1	1.3
	Ag $3d_{3/2}$	374.1	1.3
Auger parameter	a_1	725.7	…
	a_2	720.7	…
Thin film	Ag $3d_{5/2}$	368.1	1.16
	Ag $3d_{3/2}$	374.1	1.16
	Mg 1s	1303.9	1.78
	O 1s (MgO)	530.3	1.9
	O 1s (H_2O)	532.9	2.9
Auger parameter	a_1	725.7	…
	a_2	720.7	…

spectra showed a surface free from contaminants with oxygen and carbon not present on the surface. The Ag 3d peak positions (Table I) closely agreed with reference values.[21] Auger parameters for Ag are also displayed and compared to reference values, to check for potential surface charge effects introduced by the MgO insulating film deposition. The modified Auger parameters outlined by Gaarenstroom and Winograd.[22] are calculated for Ag as follows:

$$a_1 = E_b + E_{k5},$$

$$a_2 = E_b + E_{k4},$$

where E_b is the binding energy (BE) of the Ag $3d_{5/2}$ core region and $E_{k5,k4}$ are the kinetic energies of the Ag $M_5N_{45}N_{45}$ and Ag $M_4N_{45}N_{45}$ Auger peaks, respectively. The clean Ag Auger parameters (Table I) were also in close agreement with reference data.[21] Surface crystallographic ordering was confirmed by a sharp (1×1) LEED pattern: such a pattern at electron energy of 140 eV is shown in Fig. 2(a).

After MgO film deposition, a slightly more diffuse (1×1) LEED pattern with identical spot spacing was observed [Fig. 2(b)]. The expected Mg and O peaks appeared in XPS, with the Ag substrate peaks still intense. These results are consistent with either (a) MgO islands on Ag, (b) an ultra-thin amorphous MgO film or (c) an ultra-thin epitaxial MgO film. Because the LEED spots remains clear and distinct down to low electron energies (below 70 eV), with similar intensity on both clean and MgO-covered surfaces, we discount (b). A typical AFM topograph is shown in Fig. 3(a). The whole surface is densely decorated with flat islands of lateral size several tens of nm and average height around 0.5 nm. The curved line with two cusps is a surface step-bunch on the Ag substrate (average height 2 nm). The density of islands is higher at edge of the upper terrace, which we suggest is caused by the Erlich–Schwoebel barrier[23–25] for Mg atoms migrating on the Ag surface during growth, leading to higher nucleation density on the upper edge of the step bunch.[26] The overall surface coverage by the islands is approximately 80%. A typical LFM image is shown in Fig. 3(b). The color scale represents lateral force, which depends on the frictional properties of the material with which the AFM tip is in contact. Height contours are overlain on this image (black is low, white is high). There is a strong correlation between the frictional force and the height, which shows that the islands have different frictional properties to the "valleys." The simplest explanation is that the islands are MgO and some Ag substrate remains uncovered. We therefore discount option (c) and conclude that the deposition protocol has resulted in 80% coverage of

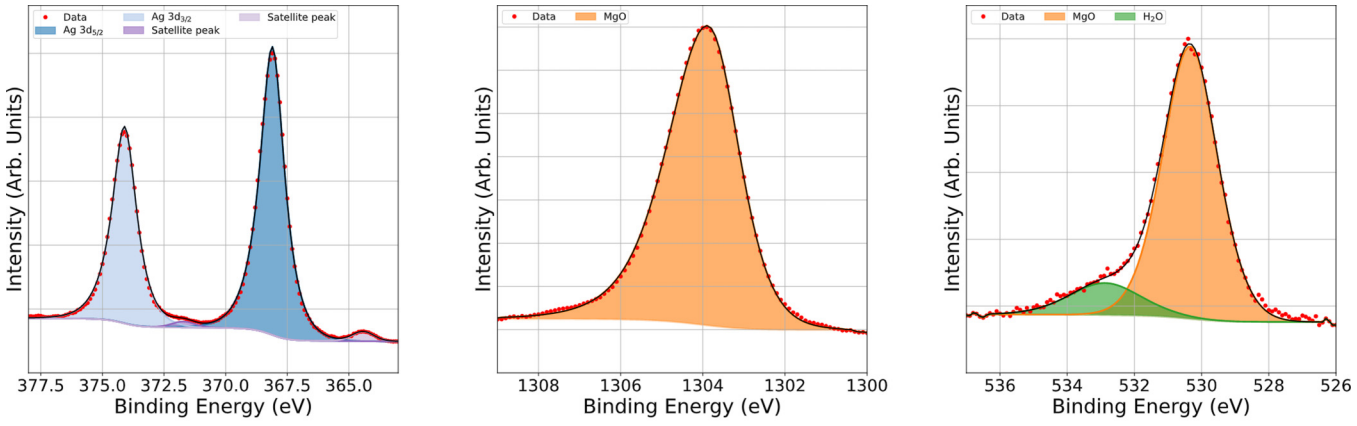

FIG. 1. XPS core region spectra of (a) Ag 3d, (b) Mg 1s, and (c) O 1s after deposition of the MgO film. Fitted components are distinguished by color.

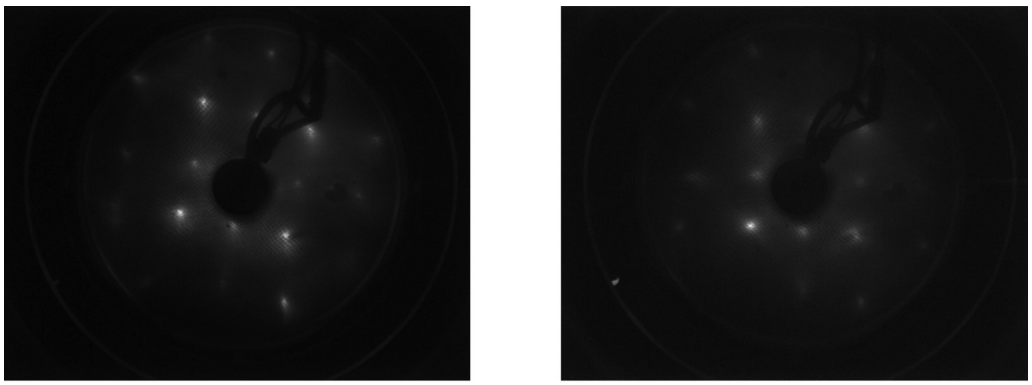

(a) (b)

FIG. 2. (1 × 1) LEED patterns at electron energy of 140 eV before (a) and after (b) ultra-thin MgO film deposition.

epitaxial MgO islands with monolayer or few-monolayer heights. The epitaxial strain for MgO on Ag is 3.1% so the film could be partially relaxed, leading to the more diffuse LEED pattern. This incomplete coverage may also explain the lower WF shift observed, compared to the predicted −1.16 eV,[8] owing to UPS measuring the average WF value over the sampling area. This growth mode is consistent with the work of Ouvrard *et al.*,[27] where deposition at low temperatures (around 373 K) resulted in a high density of MgO islands due to the small surface mobility.

The Ag 3d spectrum shown in Fig. 1(a) comprises a single doublet component and indicates that there was no formation of Ag (sub-) oxide in the substrate. The Mg 1s XPS spectrum, shown in Fig. 1(b), likewise displays one distinct peak at the BE of 1303.9 eV: this is consistent with MgO, agreeing with previously reported data.[28] The lack of a component at 1303 eV strongly suggests that there is no metallic Mg present. The asymmetry of the Mg 1s peak we can attribute to inelastic losses from multiple surface phonon excitation, rather than any chemically shifted

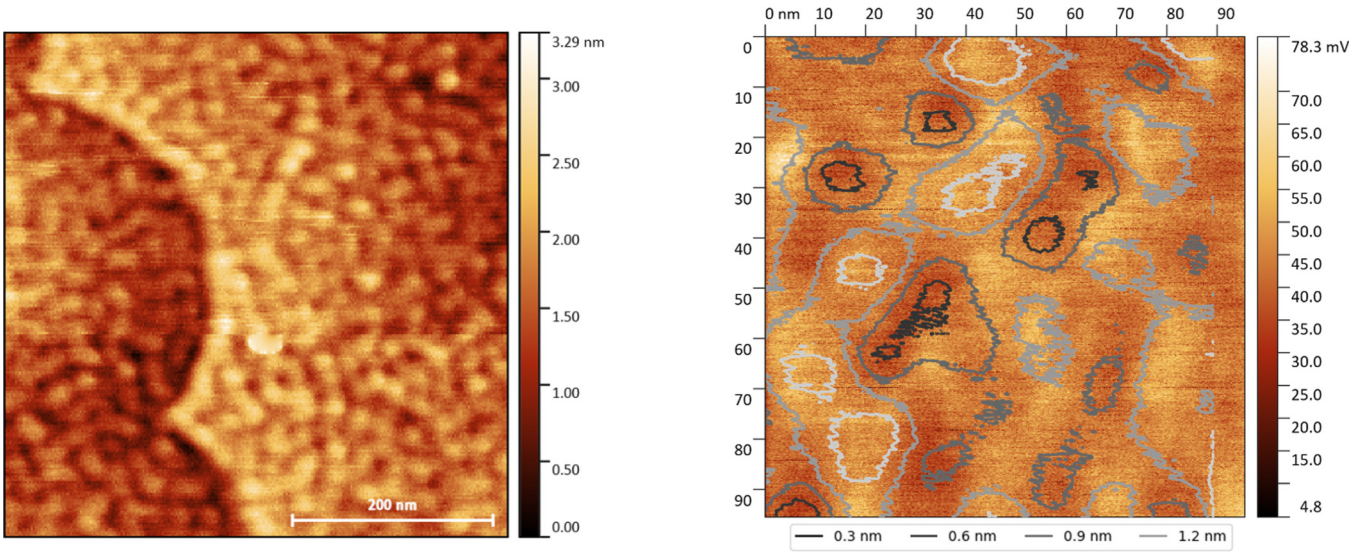

(a) (b)

FIG. 3. (a) 0.5 × 0.5 μm^2 AFM topograph. (b) 100 × 100 nm^2 LFM image overlaid with a contour height map (0.3, 0.6, 0.9, and 1.2 nm represented by black and increasingly lighter gray lines, respectively). Vertical scale represents the lateral force.

TABLE II. Measured QE_{ab} measurements of the the Ag(100) substrate and MgO/Ag(100) film. WF was measured for MgO/Ag(100) film and reference data was used for Ag(100).

	WF (eV)	QE_{ab}
Clean Ag(100)	4.36 ± 0.05[a]	1.12×10^{-4}
MgO/Ag(100)	3.40 ± 0.10	9.22×10^{-4}

[a]Reference 32.

components (a full discussion of this effect will be given in a future paper). Conversely, the O 1s region has two components, shown in Fig. 1(c). The more prominent peak with a BE of 530.3 eV is assigned, using reference spectra,[29] to be the MgO contribution. The smaller peak with a BE of 532.9 eV is from oxide contamination in the form of adsorbed H_2O. Altieri *et al.*[30] showed that MgO films have a high chemical activity toward H_2O dissociative chemisorption. The source of the H_2O is most likely during the introduction of the O_2 during Mg deposition since the gas line cannot be thoroughly baked.

The thickness of the MgO layer was estimated to be 4.5 ± 0.3 Å using the thickogram method outlined by Cumpson,[31] where the peak intensities of the Mg 1s (overlayer), Ag 3d (substrate) and the attenuation length of electrons through the overlayer at distinct kinetic energies are evaluated. Overall, the XPS spectra suggest a stoichiometric MgO layer with a mean thickness around 1.5 monolayers, which is consistent with the growth mode data obtained from LEED and AFM/LFM.

B. Photocathode properties

Table II shows the measured work function of the MgO/Ag(100) film photocathode, compared to the Ag(100) reference value of 4.36 ± 0.05 eV.[32] The application of the MgO film induced a significant reduction of 0.96 ± 0.11 eV in WF to a measured value of 3.40 ± 0.10 eV.

As expected, the reduction in the WF has a significant effect on the photoemissive properties of the Ag(100) photocathode. First, QE_{ab}, Table II, for Ag(100) at 266 nm strongly agrees with the theoretical value of 1.1×10^{-4} calculated by Camino *et al.*,[33] and the introduction of the ultra-thin MgO film greatly increased the QE by a factor of 8.4. The reduction in the WF will also increase the excess energy in any photoemission event, as can be seen in Eq. (1). This is shown in Fig. 4 where the measured MTE for the bare Ag(100) photocathode and the MgO enhanced Ag(100) photocathode under different illumination wavelengths are presented. The MTE was measured at room temperature for both

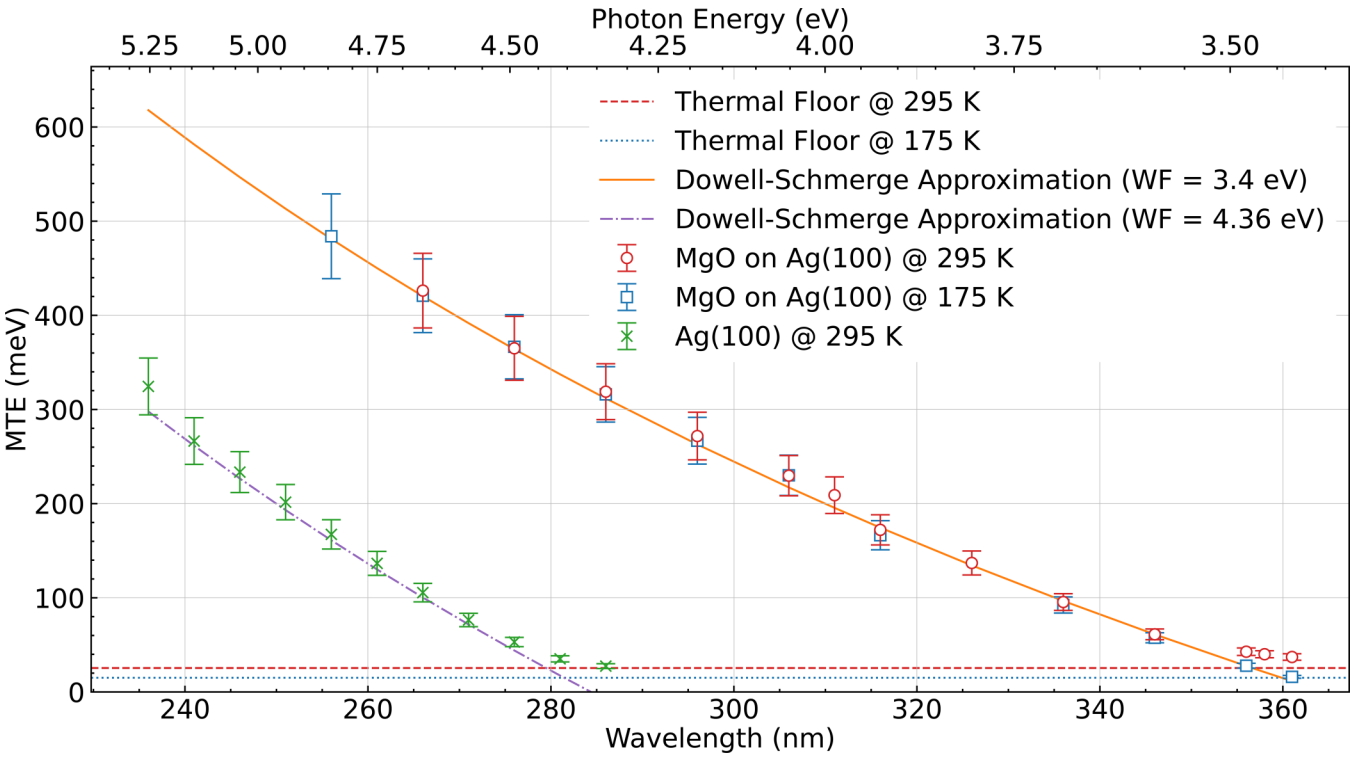

FIG. 4. MTE measurements for the Ag(100) photocathode (green points) and MgO enhanced photocathode at room temperature (red points) and 175 K (blue points). The red and blue dashed lines represent the MTE thermal floor, defined by $k_B T$, at room temperature and at 175 K. The orange and purple line show the predicted MTE following the model in Eq. (1).

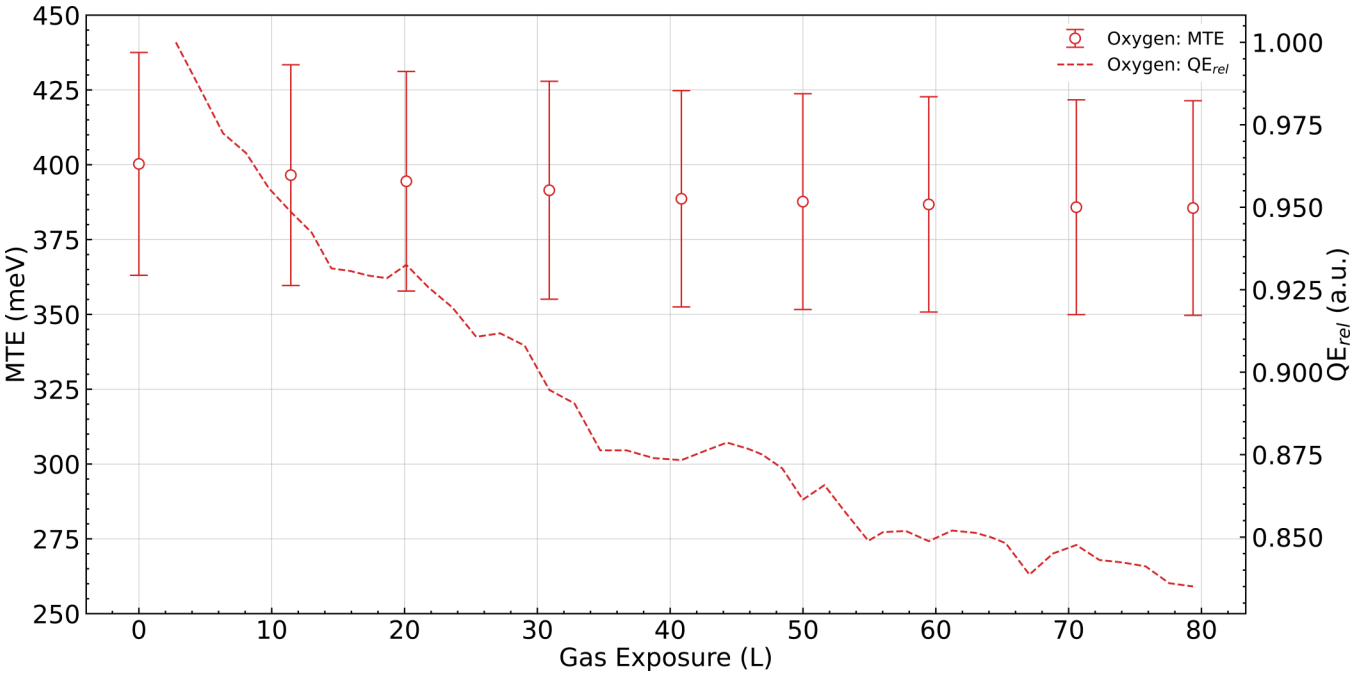

FIG. 5. MTE and QE_{rel} degradation of the MgO-enhanced Ag(100) photocathode when exposed to O_2.

samples and a second set of measurements were taken at 175 K for MgO/Ag(100). All data points have an experimental error of $\pm 10\%$.[19] Overall, the data show the direct dependence of the MTE on the excess energy and exhibit excellent agreement with Eq. (1).

At an incident wavelength of 266 nm (the third harmonic of a Ti:Sapp laser commonly used to drive a photoinjector), the measured MTE increased from 105 to 426 meV when comparing the room temperature measurements for Ag(100) and MgO/Ag(100). When cryogenically cooled, MgO/Ag(100) showed a slight reduction to 420 meV. At threshold emission, a wavelength of 361 nm, the sample demonstrated a MTE of 37 meV which reduced to 16 meV when cooled to 175 K. This is commensurate with the minimum energy determined by the temperature of the system (k_BT), 25 meV and 15 meV at room temperature and 175 K, respectively. The bare Ag(100) sample achieved a minimum value of 29 meV at a threshold wavelength of 286 nm. The data also demonstrate a substantial broadening in the spectral response of the modified surface compared to the bare metal.

A degradation experiment was conducted in the TESS facility where a typical poisoning gas, O_2, was admitted into the vacuum chamber to progressively degrade the photocathode in a controlled manner. The chamber pressure increased from its base of 5×10^{-11} to 6×10^{-9} mbar, representing a partial pressure of 5.95×10^{-9} mbar of O_2. During exposure, the MTE and pressure were monitored. A relative QE (QE_{rel}) measurement was extracted by considering the photoemission footprint image intensity and dividing by the calibrated gain parameters of the multi channel plate, the measured average power, and the exposure time of image.

Figure 5 shows the measured MTE and QE_{rel} at 266 nm when exposed to O_2. The photocathode was exposed to around 79 L of O_2 gas which drove a drop of 17% drop in QE_{rel}. Oxygen exposure also slightly reduces the MTE, from 400 meV (clean) to 387 meV (79 L). This trend, discernible despite the error bars, is expected as the QE reduces.

IV. DISCUSSION

As previously discussed, the WF shift induced by one MgO monolayer has been predicted to be around -0.94 eV[7] and potentially up to -1.16 eV.[8] Experimentally, König *et al.*[34] observed a shift of -0.5 and -1.2 eV, when measured using Kelvin probe force microscopy and field emission resonances, respectively. The WF shift observed in our samples of -0.96 ± 0.1 eV is within theoretical expectation and comparable to the reported values of König *et al.*

The observed increase in QE_{ab}, at 266 nm, by over $8\times$ relative to Ag is a result of the reduction in the WF. Therefore, the increase in the MTE relative to the bare Ag photocathode is also expected. At threshold emission, both the bare Ag(100) and the MgO film achieved minimum energy constrained by the thermal energy of the system. Furthermore, cryogenically cooling the MgO enhanced Ag photocathode to 175 K reduced the measured threshold MTE to 16 meV. This strongly indicates that the growth of the film did not introduce additional surface roughness and is not contributing to the MTE in a significant manner. This is consistent with the AFM topography observed, where Ag step bunch heights and starting

surface roughness are both are larger than MgO island heights of 1–2 monolayers.

When exposed to 13 L of O_2, the MgO/Ag(100) photocathode had a QE_{rel} drop of 6.2%. After a further 79 L, QE_{rel} fell by a total of 16%. Previous work conducted on TESS by Soomary *et al.*[35] investigated the stability of the same clean Ag(100) photocathode using the same experimental setup. They observed a reduction of 6.2% in QE_{rel} after a much smaller exposure of 0.24 L. Our results highlight the great improvement in inertness of the MgO-enhanced photocathode. The unexpected decay of QE_{rel} by 16% can be attributed to reduced photoemission from the exposed Ag(100) due to disordered adsorption of O_2.[36] Increasing the coverage of the MgO film should result in further improvements to the robustness of the photocathode, but possibly causing a drop of QE_{ab} from electron attenuation in thicker MgO islands. Optimization of the film growth recipe could allow fuller coverage of ultra-thin MgO.

V. CONCLUSION

We have shown experimentally that the inclusion of an ultra-thin MgO film dramatically enhances the photoemissive properties of a Ag(100) photocathode. The MgO-enhanced photocathode exhibited a WF reduction close to 1 eV relative to clean Ag(100), in agreement with previous theoretical and experimental data.[34] Furthermore, an increase in QE to 9.22×10^{-4} at 266 nm was observed, which is in line with theoretical predictions[8] and a factor of 8 increase relative to clean Ag(100). The WF reduction also demonstrates its potential as a UV-A sensor with a measurable photocurrent response at wavelengths below 360 nm. Finally, the O_2 degradation experiment also suggests the inclusion of the MgO film enhanced the robustness of the photocathodes against gas exposure, in turn potentially improving its operational lifetime of in an accelerator environment.

The strong potential for MgO-enhanced Ag(100) photocathodes in a range of applications has been clearly demonstrated. Further optimization of the MgO growth could improve surface coverage without significantly increasing average MgO thickness or surface roughness. Experiments on other low-index Ag surfaces would also be valuable to compare with first-principles calculations and to understand the effects of MgO on polycrystalline Ag.

ACKNOWLEDGMENTS

Christopher Benjamin is supported by a Warwick Collaborative Postgraduate Research Scholarship.

AUTHOR DECLARATIONS

Conflict of Interest

The authors have no conflicts to disclose.

Author Contributions

C. Benjamin: Formal analysis (equal); Investigation (lead); Methodology (equal); Visualization (equal); Writing – original draft (lead). **H. M. Churn:** Formal analysis (equal); Investigation (equal); Methodology (equal); Visualization (equal); Writing – review & editing (equal). **T. J. Rehaag:** Investigation (equal); Writing – review & editing (equal). **L. A. J. Soomary:** Investigation (equal). **C. P. Welsch:** Supervision (equal). **L. B. Jones:** Methodology (equal); Supervision (equal); Writing – review & editing (equal). **T. C. Q. Noakes:** Funding acquisition (equal); Supervision (equal); Writing – review & editing (supporting). **G. R. Bell:** Funding acquisition (equal); Supervision (equal); Writing – review & editing (equal).

DATA AVAILABILITY

The data that support the findings of this study are available from the corresponding author upon reasonable request.

REFERENCES

[1]K. L. Jensen, P. G. O'Shea, D. W. Feldman, and N. A. Moody, "Theoretical model of the intrinsic emittance of a photocathode," Appl. Phys. Lett. **89**, 224103 (2006).
[2]D. Dowell, I. Bazarov, B. Dunham, K. Harkay, C. Hernandez-Garcia, R. Legg, H. Padmore, T. Rao, J. Smedley, and W. Wan, "Cathode R&D for future light sources," Nucl. Instrum. Methods Phys. Res. Sect. A **622**, 685–697 (2010).
[3]D. A. Dimitrov, G. I. Bell, J. Smedley, I. Ben-Zvi, J. Feng, S. Karkare, and H. A. Padmore, "Modeling quantum yield, emittance, and surface roughness effects from metallic photocathodes," J. Appl. Phys. **122**, 165303 (2017).
[4]I. Bazarov, L. Cultrera, A. Bartnik, B. Dunham, S. Karkare, Y. Li, X. Liu, J. Maxson, and W. Roussel, "Thermal emittance measurements of a cesium potassium antimonide photocathode," Appl. Phys. Lett. **98**, 224101 (2011).
[5]D. H. Dowell and J. F. Schmerge, "Quantum efficiency and thermal emittance of metal photocathodes," Phys. Rev. ST Accel. Beams **12**, 074201 (2009).
[6]P. Musumeci, J. Giner Navarro, J. Rosenzweig, L. Cultrera, I. Bazarov, J. Maxson, S. Karkare, and H. Padmore, "Advances in bright electron sources," Nucl. Instrum. Methods Phys. Res. Sect. A **907**, 209–220 (2018).
[7]S. Prada, U. Martinez, and G. Pacchioni, "Work function changes induced by deposition of ultrathin dielectric films on metals: A theoretical analysis," Phys. Rev. B **78**, 235423 (2008).
[8]V. Chang, T. C. Q. Noakes, and N. M. Harrison, "Work function and quantum efficiency study of metal oxide thin films on Ag(100)," Phys. Rev. B **97**, 155436 (2018).
[9]J. Goniakowski and C. Noguera, "Polarization and rumpling in oxide monolayers deposited on metallic substrates," Phys. Rev. B **79**, 155433 (2009).
[10]T. Jaouen, G. Jézéquel, G. Delhaye, B. Lépine, P. Turban, and P. Schieffer, "Work function shifts, Schottky barrier height, and ionization potential determination of thin MgO films on Ag(001)," Appl. Phys. Lett. **97**, 232104 (2010).
[11]R. C. Ropp, "Group 16 (O, S, Se, Te) alkaline earth compounds," in *Encyclopedia of the Alkaline Earth Compounds* (Elsevier, Amsterdam, 2013), pp. 105197, Chap. 3.
[12]D. Vartsky, A. Roy, A. Coimbra, S. Shchemelinin, I. Israelashvili, L. Arazi, E. Erdal, and A. Breskin, "CsI-photocathode *in-situ* monitoring system in gaseous and noble-liquid photomultipliers," J. Instrum. **14**, T07006 (2019).
[13]M. Baruzzo, C. Chatterjee, P. Ciliberti, S. Dalla Torre, S. Dasgupta, B. Gobbo, M. Gregori, G. Hamar, S. Levorato, G. Menon, C. Santos, F. Tessarotto, P. Triloki, D. Varga, and Y. Zhao, "Direct measurements of the properties of thick-gem reflective photocathodes," Nucl. Instrum. Methods Phys. Res. Sect. A **972**, 164099 (2020).
[14]M. Spangenberg, J. I. Bryant, S. J. Gibson, P. J. Mousley, Y. Ramachers, and G. R. Bell, "Ultraviolet absorption of contaminants in water," Sci. Rep. **11**, 3682 (2021).
[15]R. Musket, W. McLean, C. Colmenares, D. Makowiecki, and W. Siekhaus, "Preparation of atomically clean surfaces of selected elements: A review," Appl. Surface Sci. **10**, 143–207 (1982).
[16]P. Ruffieux, P. Schwaller, O. Gröning, L. Schlapbach, P. Gröning, Q. C. Herd, D. Funnemann, and J. Westermann, "Experimental determination of the

transmission factor for the omicron EA125 electron analyzer," Rev. Sci. Instrum. **71**, 3634 (2000).
[17]N. Fairley, V. Fernandez, M. Richard-Plouet, C. Guillot-Deudon, J. Walton, E. Smith, D. Flahaut, M. Greiner, M. Biesinger, S. Tougaard, D. Morgan, and J. Baltrusaitis, "Systematic and collaborative approach to problem solving using X-ray photoelectron spectroscopy," Appl. Surface Sci. Adv. **5**, 100112 (2021).
[18]L. B. Jones, R. Cash, B. Fell, K. Middleman, B. Militsyn, T. Noakes, D. Gorshkov, H. Scheibler, and A. Terekhov, "The commissioning of tess: An experimental facility for measuring the electron energy distribution from photocathodes," in *Proceedings of FEL'13* (JACoW Publishing, Geneva, 2013), pp. 290–293.
[19]L. Jones, D. Juarez-Lopez, H. Scheibler, A. Terekhov, B. Militsyn, C. Welsch, and T. Noakes, "The measurement of photocathode transverse energy distribution curves (TEDC) using the transverse energy spread spectrometer (TESS) experimental system," Rev. Sci. Instrum. (to be published).
[20]L. B. Jones, H. E. Scheibler, D. V. Gorshkov, A. S. Terekhov, B. L. Militsyn, and T. C. Q. Noakes, "Evolution of the transverse and longitudinal energy distributions of electrons emitted from a GaAsP photocathode as a function of its degradation state," J. Appl. Phys. **121**, 225703 (2017).
[21]A. M. Ferraria, A. P. Carapeto, and A. M. Botelho do Rego, "X-ray photoelectron spectroscopy: Silver salts revisited," Vacuum **86**, 1988–1991 (2012).
[22]S. W. Gaarenstroom and N. Winograd, "Initial and final state effects in the ESCA spectra of cadmium and silver oxides," J. Chem. Phys. **67**, 3500–3506 (1977).
[23]R. L. Schwoebel and E. J. Shipsey, "Step motion on crystal surfaces," J. Appl. Phys. **37**, 3682–3686 (1966).
[24]R. L. Schwoebel, "Step motion on crystal surfaces. II," J. Appl. Phys. **40**, 614–618 (1969).
[25]G. Ehrlich and F. G. Hudda, "Atomic view of surface self-diffusion: Tungsten on tungsten," J. Chem. Phys. **44**, 1039–1049 (1966).
[26]K. Morgenstern, "Fast scanning tunnelling microscopy as a tool to understand changes on metal surfaces: From nanostructures to single atoms," Phys. Stat. Sol. (B) **242**, 773–796 (2005).
[27]A. Ouvrard, J. Niebauer, A. Ghalgaoui, C. Barth, C. R. Henry, and B. Bourguignon, "Characterization of thin MgO films on Ag(001) by low-energy electron diffraction and scanning tunneling microscopy," J. Phys. Chem. C **115**, 8034–8041 (2011).
[28]H. Seyama and M. Soma, "X-ray photoelectron spectroscopic study of montmorillonite containing exchangeable divalent cations," J. Chem. Soc. Faraday Trans. 1 **80**, 237–248 (1984).
[29]S. Ardizzone, C. Bianchi, M. Fadoni, and B. Vercelli, "Magnesium salts and oxide: An XPS overview," Appl. Surf. Sci. **119**, 253–259 (1997).
[30]S. Altieri, L. H. Tjeng, and G. A. Sawatzky, "Electronic structure and chemical reactivity of oxide-metal interfaces: MgO(100)/Ag(100)," Phys. Rev. B **61**, 16948–16955 (2000).
[31]P. J. Cumpson, "The thickogram: A method for easy film thickness measurement in XPS," Surf. Interface Anal. **29**, 403–406 (2000).
[32]G. N. Derry, M. E. Kern, and E. H. Worth, "Recommended values of clean metal surface work functions," J. Vac. Sci. Technol. A **33**, 060801 (2015).
[33]B. Camino, T. Noakes, M. Surman, E. Seddon, and N. Harrison, "Photoemission simulation for photocathode design: Theory and application to copper and silver surfaces," Comput. Mater. Sci. **122**, 331–340 (2016).
[34]T. König, G. H. Simon, H.-P. Rust, and M. Heyde, "Work function measurements of thin oxide films on metals—MgO on Ag(001)," J. Phys. Chem. C **113**, 11301–11305 (2009).
[35]L. A. J. Soomary, L. B. Jones, T. C. Q. Noakes, and C. P. Welsch, "Controlled degradation by oxygen exposure in the performance of a Ag (100) single-crystal photocathode," in *Proceedings of IPAC'21* (JACoW Publishing, Geneva, 2021), pp. 2856–2859.
[36]H. Engelhardt and D. Menzel, "Adsorption of oxygen on silver single crystal surfaces," Surf. Sci. **57**, 591–618 (1976).